International Journal of Advances in Engineering and Management (IJAEM)
Volume 3, Issue 9 Sep 2021, pp: 654-671 www.ijaem.net ISSN: 2395-5252

Development of Sun Tracking Solar Panel to Maximize Energy Generated In Satellites

Sandeep Kumar[1], Er.Ajay Kumar[2]

[1]*M.Tech. Student of Electrical and Electronics Engineering, Department of Electrical and Electronics Engineering, BSEC(SHUBHARTI UNIVERSITY), Meerut-250004, U.P., INDIA*

[2]*Assistant Professor of Electrical and Electronics Engineering, Department of Electrical and Electronics Engineering, BSEC(SHUBHARTI UNIVERSITY), Meerut-250004, U.P., INDIA*

Submitted: 01-09-2021 Revised: 09-09-2021 Accepted: 12-09-2021

ABSTRACT :- With the growing number of satellite launches, particularly in LEO, optical tracking can provide a practical way to improve tracking precision and availability. Active illumination systems in space, such as LED payloads, can significantly improve optical observations. extending the observability interval to the duration of the eclipse and conducting optimum flash sequences for identification, orbit determination, attitude reconstruction, and low data rate communicationIn this work, the basic features of LED panels for optical tracking deployed on small satellite platforms (and, in particular, nano-satellite platforms) are described, as well as the design drivers. The performance is evaluated using Sun-Synchronous (at 700 km altitude) and International Space Station (at 400 km altitude) orbits, with the ground segment and optical connection budget reference design based on a conventional university space debris monitoring station architecture. The benefits of adopting various observation techniques and the range of flashing patterns are also discussed in the paper.

The LEDSAT 1U CubeSat is utilised as a study case for examples of LED payloads and related operations that are documented and explained in this work, with the goal of proving the usefulness of an LED-based payload for observation and tracking.

Key words:- Satellites, CubeSats, optical, tracking, LEDs.

1.1 INTRODUCTION

A growing number of scholars around the world are focusing on the development of renewable energy. When compared to fossil fuels, renewable energy sources are more environmentally friendly and sustainable fuels[1,3] Solar and wind energy are examples of renewable energy sources. The desire to use renewable energy rather than fossil fuels has grown, and numerous countries have boosted their solar energy reliance. Figure 1 depicts the total quantity of solar energy consumed worldwide in million tones of oil equivalent. From 2000 to 2016, the total amount of solar energy consumed on a global scale increased rapidly. In 2016, the highest amount of solar energy was utilised, however solar energy had only been used infrequently prior to this year. These statistics were compiled using official data from several government ministries and statistical offices [5,6]. Figure 2 depicts global solar energy gross generation in Terawatt-hours, whereas Figure 3 depicts total capacity in Megawatts. The overall capacity, generated, and consumed energy have all expanded exponentially, with solar energy capacity and utilisation growing at a pace of 29.6%. Solar photovoltaic cells, often known as solar panels, have been used to convert solar radiation into electricity for decades. Solar photovoltaic cells are a scalable technology that may be scaled up or down depending on the load size. Photovoltaic cells can be used to power small electronics or connected to form solar panels for bigger loads. Solar photovoltaic cells are a scalable technology that may be scaled up or down depending on the load size. Photovoltaic cells can be used to power small gadgets or connected to form solar panels to power bigger loads [6–7]. The panels can be grouped together to form a solar array for large-scale energy production.[4,8]

International Journal of Advances in Engineering and Management (IJAEM)
Volume 3, Issue 9 Sep 2021, pp: 654-671 www.ijaem.net ISSN: 2395-5252

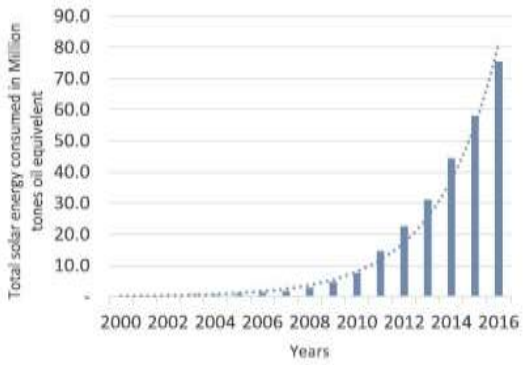

Fig-1 Total solar energy consumed in Million tones oil equivalent.

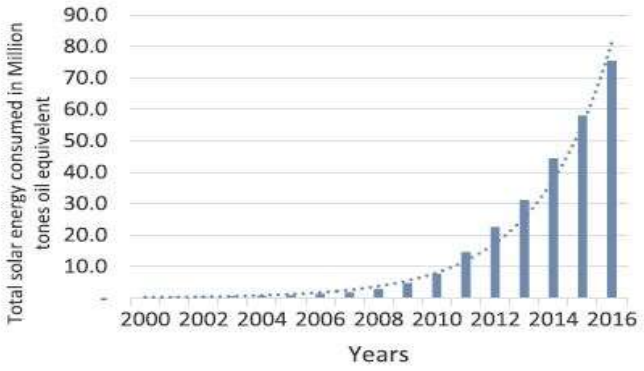

Fig-1.2 Total solar energy consumed in Million tones oil equivalent.

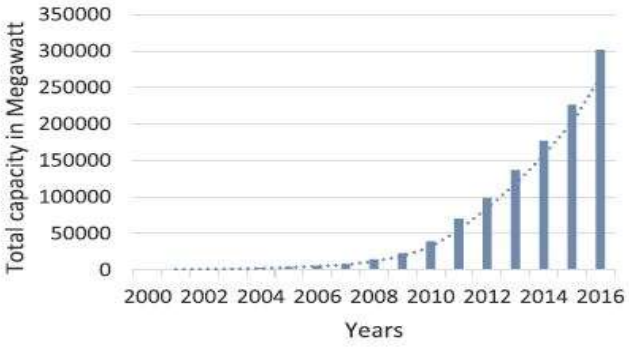

Fig-1.3 Total solar energy capacity in Megawatt.

1.2 OBJECTIVE AND WORKING PRINCIPLE OF THE CIRCUIT

The Solar Tracker Algorithm's main goal is to quickly calculate the best angle of light exposure from the sun. A pair of sensors are employed to point the light's location to the east and west. The Solar Tracker Algorithm is depicted in Fig. 2 as a flow chart. First, two sensors are installed, which detect temperature in two directions and then send the data to a Lab view application that follows a specific logic. The thermometer's output is first multiplied by a numeric value of 2400. 2400 Vo lux light intensity Because the pupil can adapt constantly in response to light, the human eye is a poor tool for detecting light intensity.

The solar tracking system's circuit is split into two pieces. The first half deals with sensors and other logical blocks that control the stepper motor, while the second part is simply a stepper motor design that moves the panel into the proper position. Figures 3 and 4 depict the logical unit of a solar tracking system and the design of a stepper motor, respectively. The following is a description of the circuit's working principle

International Journal of Advances in Engineering and Management (IJAEM)
Volume 3, Issue 9 Sep 2021, pp: 654-671 www.ijaem.net ISSN: 2395-5252

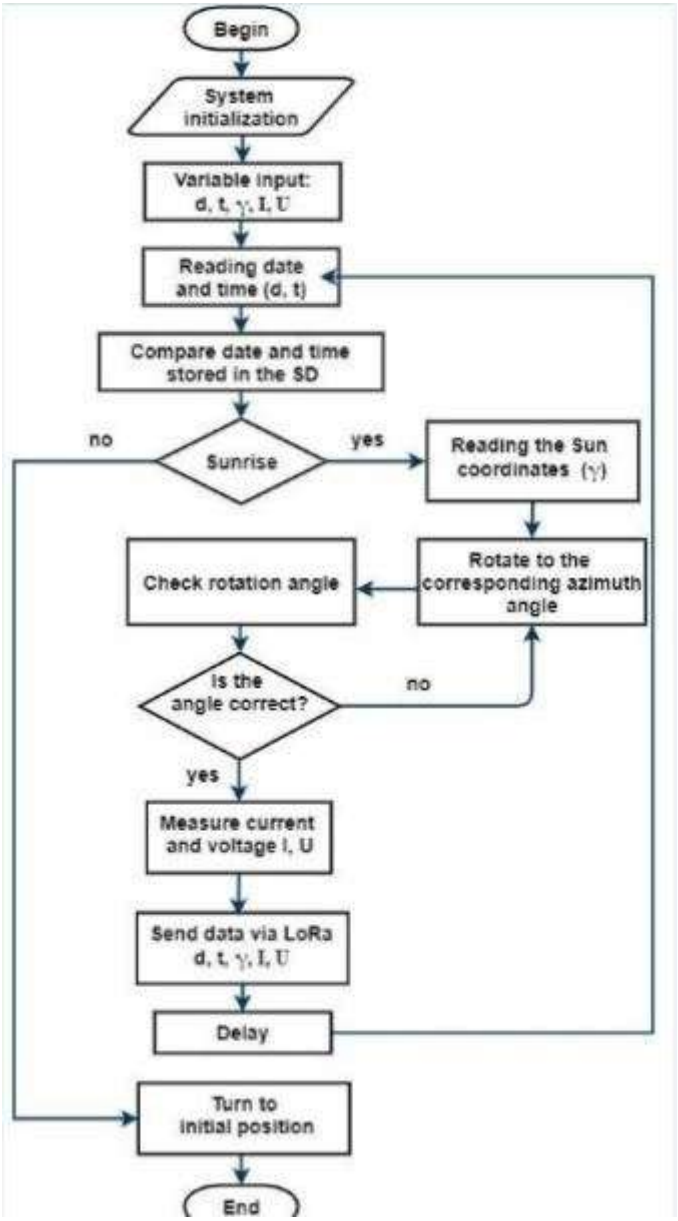

Fig-8 Logical circuit

- The thermometers' outputs are coupled to metres that display the intensity of two directions.
- With the use of wire, two sensors are installed in two directions and connected to the input data. As a sensor, two thermometers are employed.
- The thermometer's output is multiplied by a factor of 2400.
- It is determined by comparing the intensity of two directions.It is vital to compare and contrast each other.
- First the comparison is made between east intensityof the light and the west intensity of light with the help of comparison component Less (<).
- After that the output is connected to the LED which is available in the front panel of the Labview software
- If the condition is satisfied then the Led connected to it is automatically on otherwise it will turn off.
- The second part of the logical unit is as same as thefirst part of the circuit but only difference is that incase of Less (<) a Component Greater (>) is used.
- In the circuit it is seen that the intensity of the east light intensity is subtracted from the west light intensity and it is compare to the numeric value -2400

International Journal of Advances in Engineering and Management (IJAEM)
Volume 3, Issue 9 Sep 2021, pp: 654-671 www.ijaem.net ISSN: 2395-5252

- If the condition is true then the motor will move in east direction and if the condition is false then the motor will move in west direction.
- The two parts of the circuit is joined with the help of merge signal block which merges two or more signal into a single output.
- By comparing the two intensities the resultant output is send to a stepper motor
- The motor will move either clockwise or counter clockwise direction depending upon the intensities.

1.3 WORKING PRINCIPLE

A LDR is installed on each of the solar panel's four edges. A Servo motor is also installed, which rotates the panel. The solar panel will be guided by the motor towards the LDR whose resistance appears to be low, i.e. the LDR on which light is falling, in order to keep following the light. Light detectors are replaced by LDRs. Let's start with a basic understanding of how LDRs function. The light sensitive device is the LDR (Light Dependent Resistor), sometimes known as a photo resistor. The resistance lowers as light shines on it, and vice versa. This is why it is widely employed in dark or light detector circuits, as the servo will not rotate if the quantity of light falling on both LDRs is the same. The Light Dependent Resistor theory underpins solar tracking systems (LDR). Four LDRs are linked to Arduino analogue pins AO to A4 as inputs. The LDR's analogue value will be converted to digital using the built-in Analog-to-Digital Converter. The LDR's analogue value is used as an input. The Arduino serves as the controller, while the DC motor supplies the output value. LDR1 and LDR2, LDR3 and LDR4, respectively, are considered as a pair of LDRS. If one of the LDRs in a pair receives greater light intensity than the other, there will be a difference in the node voltages transmitted to the relevant Arduino channel. If one of the LDRs in each pair receives more light intensity than the other, the system will take the appropriate action.

The motor tries to move the solar panel so that the resistance of both LDRs is equal. Both resistors will receive the same amount of sunlight in this sense. If the resistance of any LDR is reduced, the panel switches to the lower resistance LDR.

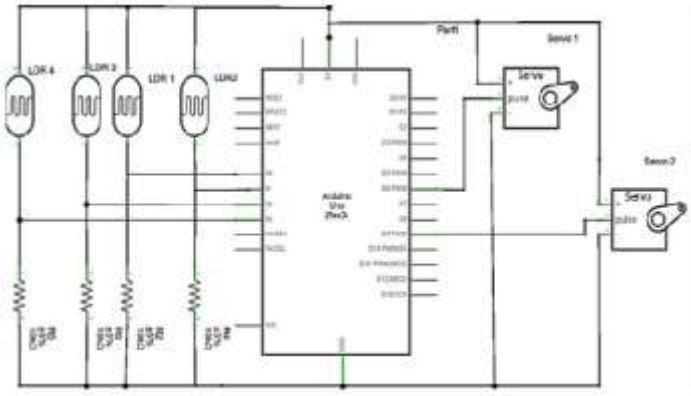

Fig- 4.5 Circuit Digram

1.4 LED-based tracking operations

The LED payloads, as stated in the Introduction section, can be used during all phases of a nanosatellite mission. The flashes that occur during commissioning and LEOP can help the spacecraft be recognised after it is deployed, especially if the satellite is part of a big cluster. The LED flashes help increase orbit determination precision during normal operations. While attempting to distinguish distinct patterns allocated to LED payloads on different faces, when permitting the collection and refinement of celestial coordinates, as well as the precision of attitude determination. If the telemetry link fails, the LEDs can act as a backup, low-data-rate data transmission system, completing a critical task of a spacecraft safe mode. Finally, the satellite's Post-Mission Disposal (PMD) can use LEDs to accelerate battery passivation by allowing LED payloads with a higher duty cycle to reduce the spacecraft's electric energy storage.

International Journal of Advances in Engineering and Management (IJAEM)
Volume 3, Issue 9 Sep 2021, pp: 654-671 www.ijaem.net ISSN: 2395-5252

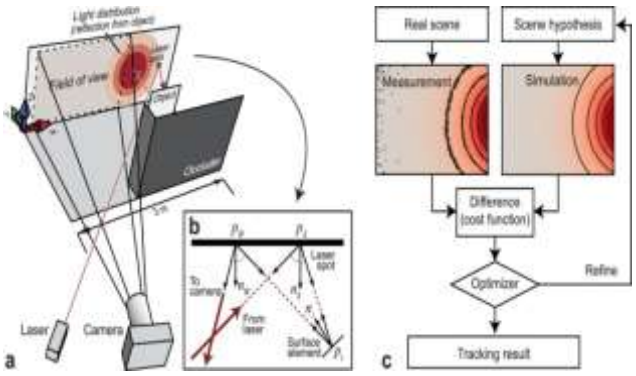

Fig- 4.7 LED-based tracking operations

1.5 Spacecraft early recognition

The satellite could perform identifier LED sequences shortly after launch and during LEOP. When satellites are deployed in big clusters, this feature will be essential. In this circumstance, less-than-accurate TLEs may cause a satellite to be confused with another from the same cluster. Misidentification can hinder the observability of satellite characteristics during the mission's early phase, preventing communication with the satellite for days or weeks and preventing mission-saving manoeuvres from being performed on time. Simply pre-programming the LED boards to flash with properly specified identifying flash sequences can be used to identify satellites. by confirming that all of the sequences used by satellites in the same cluster have a low crosscorrelation. Different Morse letters, for example, can be applied and examined [8,10], as well as orthogonal patterns [36]. Because the satellite TLE will be known with limited precision, the identification work is primarily focused on the sidereal rate observation technique. Identification processes will be performed on LEDSAT shortly after deployment [10]. Because the satellite will most likely be launched in a small group (as is customary for ISS deployments) and without additional satellites equipped with LEDs, The efficiency of this strategy will be confirmed by recognising the immediate improvement brought about by the optical observations.

An alternation of long and short flashes will be used to optimise the identifying sequences so that they are easily identifiable. Short flashes will be used to reconstruct the satellite's celestial coordinates by detecting its relative position on the image and the background star field, while extended flashes will be utilised to quickly identify the spacecraft on telescope photos.

1.6 Orbit Determination

The examination of LED flashes over a background star field can help determine a satellite's orbit. The duration of the flashes must be optimised in order to maximise the data return from the LED sequences observations. As a general rule, flashing sequences should include both long and brief flashes,. i.e. to emerge on the sensor image as long streaks and dots. The flash length will be image, whether the analysis is done with software or by hand. The quick flashes can be used to rebuild the spacecraft's orbit almost instantly. In this situation, the LEDs optimization should focus on improving the data that can be acquired and their precision rather than discriminating a known pattern. The sidereal tracking approach can be used for orbit determination and refinement, allowing the available astrometric methodologies for space debris optical orbit determination to be applied to the acquired flashes [31]. For orbit determination. As previously stated, the sidereal tracking technique using an image sensor is the recommended observational technique for improving orbit determination.determined by crossing the satellite's orbital parameters with the sensor's properties. Long flashes are aimed at quickly identifying the presence of a satellite on a telescopic

International Journal of Advances in Engineering and Management (IJAEM)
Volume 3, Issue 9 Sep 2021, pp: 654-671 www.ijaem.net ISSN: 2395-5252

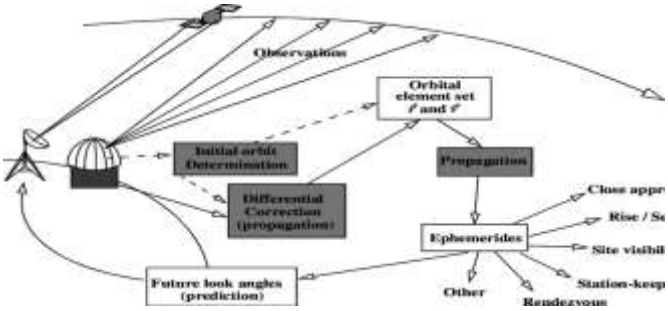

Fig- 4.8 Representation-of-Orbit-Determination

1.7 Light Communication

The LEDs can be programmed to send basic data to ground at a low rate. The data downlink can be encoded in a variety of ways. The data rate that can be achieved varies depending on the operative modes and the sensor employed. A very low data rate can be accomplished with the simplest approaches, such as the fixed mode with imaging sensors, because the flashing LEDs appear as dots and lines on a long exposure picture. As a result, the link capacity is restricted by the time it takes for the spacecraft to travel through the field of vision. CMOS and single element sensors are employed in the tracking mode. The connectivity time is prolonged in this situation to include the CubeSat's whole journey over the ground station. The use of a CMOS imaging sensor necessitates the capture of a high frame rate video in order to detect the binary flashes of the LEDs.

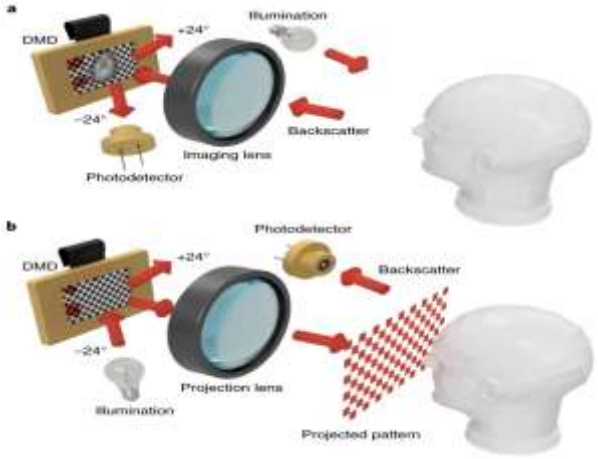

Fig- 4.9 CMOS imaging sensor

The maximum attainable data rate is 50 bits per second when using a 10ms exposure time in target tracking mode, which corresponds to a sampling rate of 100 frames per second. Table 5 shows the mean access time and data volume per passage for an average passage over mid-latitude ground.

Table 5: Mean access time over a mid-latitude ground station

Orbit	Mean access time	Data volume per passage
ISS - 400 km	570 s	28.5 kbit
SSO - 700 km	660 s	33 kbit

The LEDSAT CubeSat's experimental mode will test the downlink of dummy and housekeeping data through LEDs. Several long-range data transmission tests on the GS equipment have been done in preparation for the mission. In Anagni, the PIN photodiode was tested using an 80 mm telescope at a distance of 400 metres (Italy), While a COTS CMOS camera was tested on a 250 mm telescope at a distance of roughly 9 kilometres over Lake Bracciano's primary diameter (Italy). Figure 11[37] depicts the setup on the lakefront. A light signal was transmitted by the LEDs board, received, converted to voltage, and examined in both tests. While the first long range test demonstrated the functionality of the ground system and photodiode

International Journal of Advances in Engineering and Management (IJAEM)
Volume 3, Issue 9 Sep 2021, pp: 654-671 www.ijaem.net ISSN: 2395-5252

by receiving and decoding a K-Morse letter (as shown in Figure 12[37]), the Bracciano lake long range test consisted of transmitting binary data packets to be sampled by CMOS camera in sequential pictures, allowing 3D visualisation of the signal into the pixels array (as shown in Figure 4.12). In the worst case for atmospheric absorption, which is mitigated by the shorter distance than in the case of a satellite, the signal level displays a similar result to the link budget calculation.

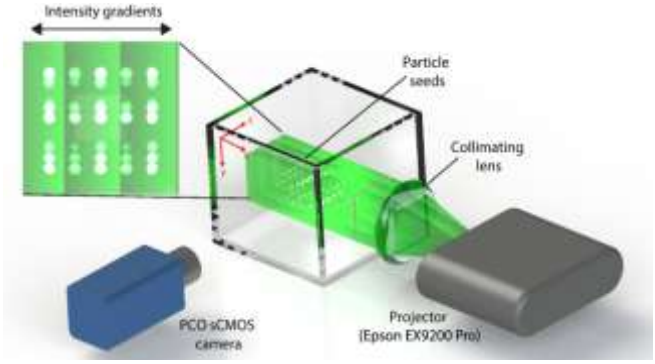

Fig- 4.10 CMOS camera

2.1 LITERATURE REVIEW

Luo et al. [18] compared the impact of neighbouring slat spacing (2.50 cm, 3.50 cm, and 4.50 cm) and slat tilt angles (30°, 45°, and 60°) in blinds on indoor thermal performance. According to the findings, under a large neighbouring slat space condition, the influence of slat angle variations on thermal performance is negligible in terms of solar heat gain and solar transmission. When the slats of experimental blinds are rotated at the same tilt degree, blinds with relatively modest gaps between neighbouring slats can block solar heat gains at significantly different levels.

Over the course of a year, **Hu et al.** [19] investigated the energy-saving potential of BIPVs (Building Integrated with Photovoltaic) mounted on Trombe walls. The best slat angles were found for six fixed angles (ranging from 0 to 75 degrees in 15 degree increments). However, instead of fenestration systems, the PV blinds were fixed on the walls, obviating the need to evaluate the daylighting behaviours for the inner rooms.

By running energy and daylighting simulations, **Li et al.** [20] examined the energy consumption performance and daylight intensity in a building with a solar shading system (i.e., blind). The slats were orientated at 30°, 60°, and 90° of tilt angles, respectively, in three layouts of the final blind designs used to facades. According to the findings, 90° of slat angle should be avoided in both vertical and horizontal blinds. Smaller angles between 0 and 60 degrees, on the other hand, are preferable in these blind systems. In order to assess the lighting conditions on the work plane in an office with blind slats,

By adjusting the slat angle in 30° increments from 0° to 90°, **Jung et al**. [21] investigated indoor illuminance, daylighting homogeneity, and glare. The findings suggest that in the spring and summer, the best tilt angle for slats was 0° (i.e., slats parallel to the horizontal plane). Because the sun's profile angle is low in the winter, The slats should be aligned at 30 degrees. **Huang et al**. [22] used the Daysim and EnergyPlus simulation software to investigate the daylighting and thermal performance of blind people. The findings show that the tilt angle of indoor blind slats has a significant impact on daylighting. Furthermore, for a building in Singapore, internal blinds positioned on the east and west facades can reduce heat gain by around 20% when compared to those mounted on the south and north facades. Under the management of the blind system, extensive research has been conducted on the indoor visual environment.

Koo et al. [23] suggested a new automated venetian blind control approach with the goal of maximising daylight benefits. The blinds are only used to protect a designated region of the room from sun glare for the occupants, so that more daylight may be introduced to the other zones in the space. Tzempelikos [24] provided a method for determining the projected view and shaded areas on windows using venetian blinds with flat and curved slat forms. The influence of slat edges on shading performance due to their thicknesses was also taken into account while the blind slats were rotated. When the blinds with arc-of-circle slats were positioned at the same tilt angles, the results showed that they performed similarly to the blinds with flat-shaped slats in terms of daylighting.

Hong et al. [25] proposed an automatic sun-tracking system for two blinds, the slats of which are controlled by 180° and 360° one-degree-of-freedom rotations, respectively. Measurement data from a real office space (i.e., test room) with the proposed blind placed under 360° rotation control, as well as a

International Journal of Advances in Engineering and Management (IJAEM)
Volume 3, Issue 9 Sep 2021, pp: 654-671 www.ijaem.net ISSN: 2395-5252

reference room with the identical conditions but 180° rotation control, were compared. The average illuminance in the reference room was only 21.86–38.86 percent of that in the test room, according to the comparison data. There is a growing amount of research focusing on energy savings in buildings that have automatic rotating blinds installed.

According to Roche [26], a fenestration system combined with an autonomously controlled blind has the potential to save a significant amount of lighting energy while also providing a pleasant visual experience.

So-Hyun Kim et al. [27] suggested a daylight responsive dimming-PV blind LED lighting system in a test room. This shading system is distinguished by the simultaneous energy savings and generation of power from electrical illumination. Controlling the slat angles of PV blinds to be perpendicular to the sun's profile angles resulted in around 35 percent energy savings and a 32 percent increase in power generation. When compared to a fixed slat angle control,

3.1 MATERIALS AND METHODOLGY

When thinking about how to build the design, the fundamental idea is to use solar power as much as feasible. The basic requirement of all expectations is to store solar energy to its maximum capacity, which leads to the development of a new solar tracking system that is self-contained. The following are the main components of this system:

- Panel of Solar Arrays
- DC Motor
- L293D Motor driver
- Microcontroller/ Arduino Board
- LDR
- Current sensor

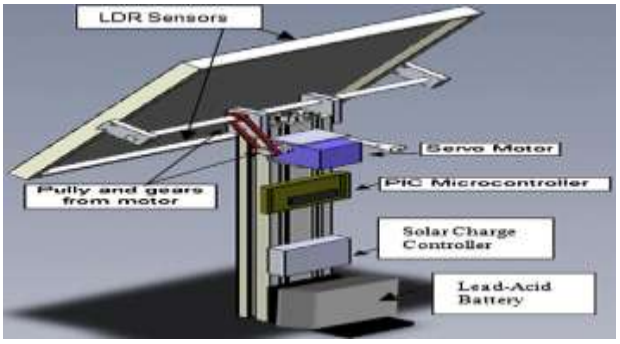

Fig-3.1 Solar tracking design/Simulator

3.2 Solar panels

Solar panels are made up of photovoltaic cells that excite electrons when photons strike them. Crystalline silicon cells or thin-film semiconductor material are used in the majority of residential applications. Monocrystalline silicon cells, in which the entire cell pack is made up of a single silicon crystal [2], are used in solar panels. The average amount of sunlight per solar panel is related to the angle of the sun with respect to the panel [5]. A solar tracking system is used to keep the angle between the sun's rays and the solar array at 90 degrees. The product of voltage under open-circuit condition (VOC) and current under short-circuit condition (ISC) is defined as the highest power for calculating electricity (ISC), and fill factor (FF).

$$P_{\max} = V_{OC} * I_{SC} * FF \quad (1)$$

The efficiency (η) is then calculated as

$$E = \frac{V_{OC} * I_{SC} * FF}{P_{in}} \quad (2)$$

3.3 DC motor and driver

When a current-carrying conductor is put in an external magnetic field, it will experience a force that is proportional to the conductor's current and the external magnetic field's intensity. The Driver is a motor module that allows you to control the direction and speed of many motors at the same time. To run a motor, you'll need some drivers that can boost the 5v voltage to 12v. The L293D IC is used to construct this motor driver. Because the L293D is the most often used H-bridge driver IC, many IC manufacturers now have H-bridge motor drivers on the market. Transistors and MOSFETs, for example, can be used to create an H-bridge. The motor's forward, reverse, left, and right directions are controlled by this IC. The 16-pin driver IC generates bidirectional currents required for changing the motor's direction at voltages ranging from 5 to 36 V. Certain applications necessitate power electronic control, which introduces harmonics into the system, and harmonic mitigation should be addressed using appropriate harmonic filters [10,11].

The L293D driver has 2 VCCs: VCC1 is +5V and VCC2 is +12V (same as motor nominal voltage). Pins IN1 and IN2 are the control pins where:

International Journal of Advances in Engineering and Management (IJAEM)
Volume 3, Issue 9 Sep 2021, pp: 654-671 www.ijaem.net ISSN: 2395-5252

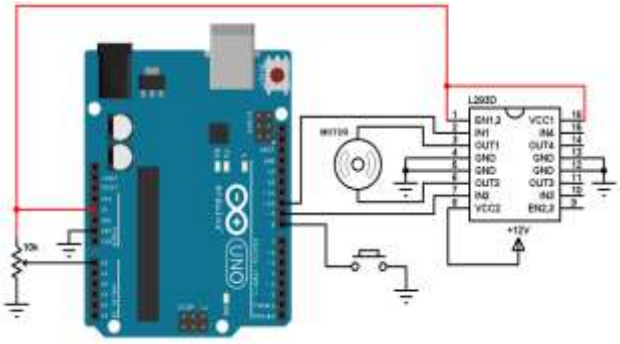

Fig-3.2 L293D IC motor driver

3.4 Microcontroller

The current state of affairs in the realm of microcontrollers may be traced back to the development of integrated circuit technology. Hundreds of thousands of transistors may now be stored on a single chip thanks to advances in technology. The ATMEGA328P microcontroller was used in the system. The microcontroller is the device's main component. The ATMEGA328P microcontroller requires a 5 V regulated voltage source. The voltage regulator '78050 aids in providing a constant 5 V supply to the microprocessor.

3.5 Light Dependent resistor (LDR)

A passive electrical component known as a Light Based Resistor or Photoresistor is essentially a resistance with a resistor that varies depending on the strength of the light. LDR is one form of resistor. The resistance of this resistor varies based on the amount of light it receives. When light levels drop on LDR, resistance rises, and vice versa. When the LDR light intensities are equivalent, a steady situation is achieved. The Sun, the major source of light's energy, travels from east to west. The degree of light intensity that falls on the LDRs varies due to the Sun's movement. The created programme calculates the difference in light intensity falling on the LDRs and subsequently rotates the solar panel to follow the light source's trail.

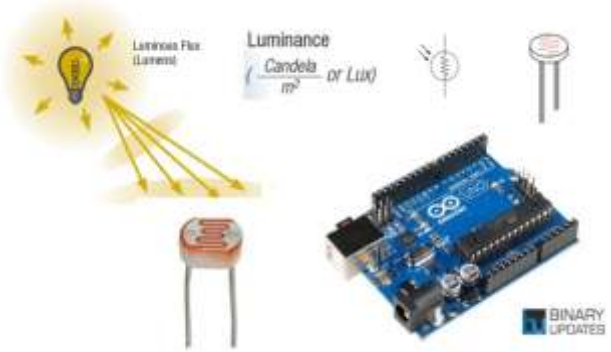

Fig-3.3 LDR with Arduino

3.6 Current sensor

When the sensor detects current, it generates a signal that is proportional to the magnitude of the current. The sensor's output can be analogue or digital in form. An ammeter can also use the initiator signal to measure current. These can also be saved for future data collecting analyses or monitored.

International Journal of Advances in Engineering and Management (IJAEM)
Volume 3, Issue 9 Sep 2021, pp: 654-671 www.ijaem.net ISSN: 2395-5252

Fig-3.4 Current sensor

4.1 SOLAR TRACING SYSTEM

Tracker systems track the sun's position, boosting solar radiation input and electrical energy output [10,11,12]. Designing, implementing, and installing these systems, on the other hand, is difficult for a variety of reasons. Before using tracker systems, a large number of measurement results are required [13–14]. These data were gathered over a lengthy period of time in order to be used in the installation of solar cells that follow the sun [9]. The information gathered is utilised to determine the optimum method for tracking the sun's position. In all instances, it is necessary to track the sun's position in order to achieve the best solar energy output. Different environmental pressures and characteristics, such as panel orientation, angle of photon incidence, time to measure the results, solar cell material, and conductivity of the solar cells,

4.2 STATEMENT OF THE PROBLEM AND HYPOTHESIS

The purpose of this research is to present and debate various types of solar tracking systems. The debate is founded on values and technologies. that was utilised to build and run these systems The differences between passive and active sun tracking systems are discussed, as well as a comparison of the control mechanisms used to drive solar tracking systems.The goal of this research is to classify solar tracking systems based on their functionality. From passive trackers to artificial intelligence-based tracking systems, many principles are given in chronological order (AI).

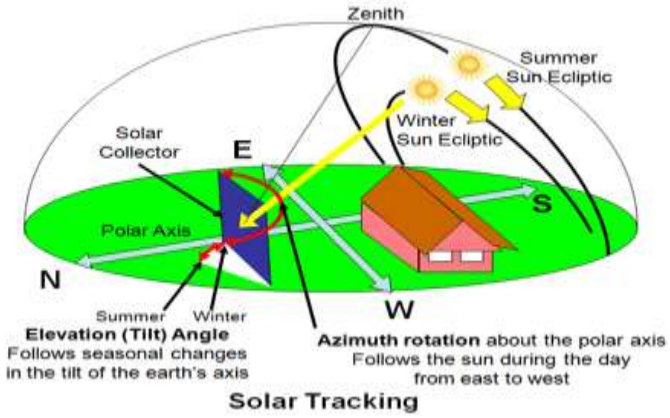

Fig-3.5 Solar Tracking system

4.3 SOLAR TRACKING SYSTEM AND MONITORING

A solar tracking system tracks the sun's position and keeps the solar photovoltaic modules at the best angle for maximum power generation. To monitor the sun efficiently, several solar tracking principles and approaches have been developed. The goal of a solar tracking system is to position solar photovoltaic modules in such a way that they can track the sun's movement across the sky and catch as much sunlight as possible. To maximise the electrical energy output, the tracker system should be situated in a position where it can obtain the best angle of incidence. Designing such a device to generate electrical energy is both fascinating and crucial. It does, however, necessitate complex mathematical calculations as well as precise observations of many solar factors.

4.4 TYPES OF SOLAR TRACKING SYSTEMS

4.4.1 Sun-tracking methods

International Journal of Advances in Engineering and Management (IJAEM)
Volume 3, Issue 9 Sep 2021, pp: 654-671 www.ijaem.net ISSN: 2395-5252

Although the existence of a solar tracker is not required for the operation of a solar panel, it does affect performance. Although solar trackers can increase the energy gain of PV arrays, there are various issues to consider when installing them, such as cost, dependability, energy consumption, maintenance, and performance.

All tracking systems have some or all of the following features.

- Single column structure or of parallel console type.
- One or two moving motors.
- Light sensing device.
- Autonomous or auxiliary energy supply.
- Light following or moving according to the calendar.
- Continuous or step-wise movement.
- Tracking all year or all year except winter.
- Orientation adjustment with/without the tilt angle adjustment.

Several sun-following technologies have been investigated and assessed in order to keep solar panels, solar concentrators, telescopes, and other solar systems parallel to the sun's beam. An ideal tracker would allow the PV cell to precisely aim towards the sun throughout the day, correcting for changes in the sun's altitude angle (during the day), latitudinal offset (during seasonal changes), and azimuth angle. Passive (mechanical) and active (electrical) trackers are the two most common types of sun-tracking systems.

4.4.2 Active solar tracking systems

Solar tracking systems that use motors, gears, and other controllers to direct photovoltaic panels toward the sun are known as active solar tracking systems. There are numerous types of active tracker systems, which can be divided into a few groups. Two solar photovoltaic modules facing opposing directions are used in the triangle tracking system, and both modules can receive equal amounts of sunshine. The simplest and cheapest tracker is the single axis tracking system; however, its efficacy is minimal because the solar module can only be pointed horizontally or vertically. Meanwhile, the photovoltaic module can be guided horizontally and vertically in the double tracking system.

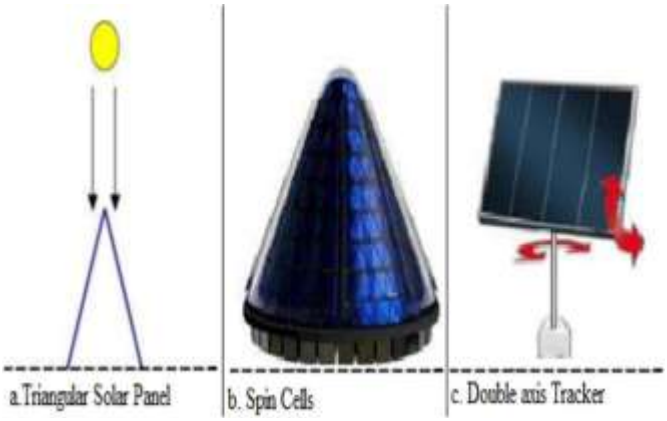

Fig-3.7 Active solar tracking system

4.4.3 Passive solar tracking systems

The temperature of the sun is used to heat a liquid that is held in canisters and adhered to the surfaces of photovoltaic modules in passive solar tracking systems. The goal is to heat this type of liquid in the canisters until it expands into a gas. The expanding gas can force the heavier liquid into the shaded canister, shifting the weight to that side of the photovoltaic module and causing it to move and spin [15]. The functioning method of passive solar tracking devices is depicted in Figure 7.

International Journal of Advances in Engineering and Management (IJAEM)
Volume 3, Issue 9 Sep 2021, pp: 654-671 www.ijaem.net ISSN: 2395-5252

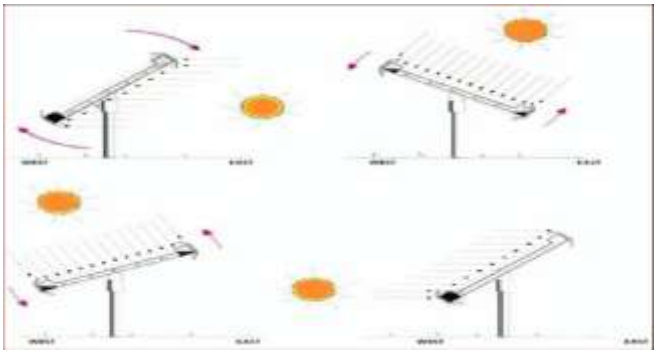

Fig-3.8 Passive solar tracking system

4.5 Operation of the solar tracker

LDRs, a solar panel, a DC motor, and a microcontroller make up the automatic solar tracking module. LDRs are installed in the solar panel's corners to detect light intensity. The basic attribute of LDRs is that they generate low resistance when the light intensity is at its highest. When the intensity of the solar beam impacting on them is at its highest, LDRs produce the least resistance. The panel is shifted by the motor linked to it in relation to the position of the sun. The solar panel is positioned in such a way that the light intensity falling on the LDRs is compared, and the motor pushes it towards the LDR with the highest light intensityThe sun is higher in the sky at midday, and the light intensity is same on both sides. The panel is stuck in this state since the motor drive isn't producing any power. The basic diagram for the automatic Solar Power Tracking System [8] is shown in Figure 4.2.

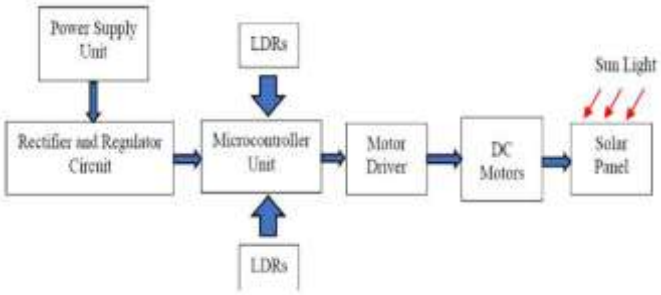

Fig. 4.2. Block Diagram of Solar Power Tracking System.

An Arduino is a microcontroller-based kit that, because to its open source hardware feature, can be purchased from a vendor or assembled at home using the components. It is mostly employed in communications as well as the control and operation of a variety of devices. The most significant advantage of Arduino is that programmes can be put directly into the device without the requirement for a hardware programmer. It's possible thanks to the Boot loader's 0.5 KB size, which allows the programme to burn into the circuit. All we have to do now is download the code and paste it into the Arduino application. The Arduino Control Circuit is shown in Figure 4.3.

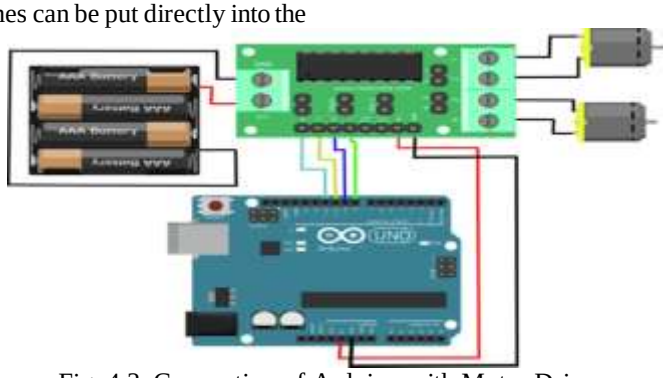

Fig. 4.3. Connection of Arduino with Motor Driver.

International Journal of Advances in Engineering and Management (IJAEM)
Volume 3, Issue 9 Sep 2021, pp: 654-671 www.ijaem.net ISSN: 2395-5252

Allow Pins are used to rotate the motor. The motor attached to the left part of the IC will revolve as stated in Table 1 for the specified inputs when Activate 1/2 is small (IP1 and IP2).

The system's performance is evaluated under two different lighting conditions: standard daylight and low light.

Table 1Motor Directional Mechanism.

IP 1	IP 2	Condition
0	0	Stop
0	1	Counter-clock wise
1	0	Clock wise
1	1	Stop

4.5.1 Normal day light condition

The LDR outputs are used by the sun tracker to compare the output voltages. When the sun moves from east to west during the day, the Analog Input 0 of the ATMEGA328P should output a higher voltage than the Analog Input 1 for monitoring the sun's rotation. The tracker achieves 3.75 rotations in the panel every 15 minutes in this mode, which is known as typical daylight.

4.5.2 Bad weather condition

On overcast days or in severe weather, the magnitude of light intensity on LDR will be lower, and hence the voltages at point [12,13] may be insufficient. The voltage differential at the junction will be smaller than the threshold value in this case, and the sun will continue to rise westward. To address this issue, a little delay is provided. Every 1.5 minutes from the junction point, the voltage input is tested. For each step rotation of the motor, the microcontroller checks the variable count ten times in a row to generate a wait signal of 15 minutes, resulting in a substantial delay.

4.5.3 Algorithm

The microcontroller is the brain of the entire solar tracking system. Through the CDS sensors, the desired light radiation is received.

The direction of the sun or the source of light can therefore be determined by equating the input radiation to the sensors [6 7].

The microcontroller then sends the desired angle of altitude and angle of elevation output signal to the motor. An algorithm must be devised in order for the microcontroller to interpret the input and respond appropriately. After that, the flow charts are translated into C and compiled using the Arduino IDE. The method's flow chart is shown in Figure 4.

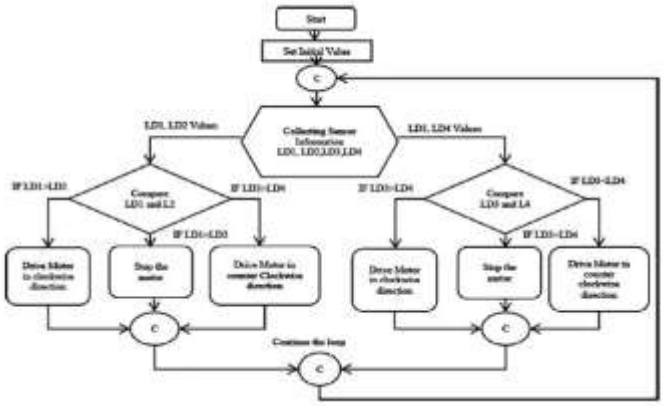

Fig. 4.4. Flowchart of the process.

5.1 EXPERIMENTAL RESULTS & CONCLUSION

The readings from the automatic sun tracking system are taken and analysed throughout normal and bad day light conditions.

Table 3 and Table 4 show the results of the observations and readings made. The Table shows different readings on different days.

International Journal of Advances in Engineering and Management (IJAEM)
Volume 3, Issue 9 Sep 2021, pp: 654-671 www.ijaem.net ISSN: 2395-5252

Table 2 System Specification.

Parameters	Specification
Weight	75 g
Diode	WG40 Bridge
Transformer	230V/12V AC
Rectifier	W04G Bridge
Filter Capacitor	1000µf & 100µf
Resistance	330 Ω, 10K X
IC Regulator	IC 7805
LDR	PG Series/ CdS
Arduino	ATmega328P
Motor	0-5V
Temperature Rang	0°C – 55°C
Solar panel	V(OC) : 11.05 VI(SC) : 10AP(Out): 10 W

Table 3 Experimental results under normal day light condition.

Time	LDR_1	LDR_2	LDR_3	LDR_4	Temp.(°c)	Fixed panel (W)	Dual Axis panel (W)
07:00 AM	46	74	158	75	25	2.2	6.02
08:00 AM	45	76	164	76	26	3.65	7.88
09:00 AM	47	71	170	66	28	6.7	8.56
10:00 AM	48	69	163	64	29	7.35	8.78
11:00 AM	45	56	165	51	29	7.9	8.47
12:00 PM	42	48	45	50	30	8.82	9.6
01:00 PM	47	45	51	47	31	8.85	9.34
02:00 PM	166	160	54	160	32	8.62	9.1
03:00 PM	173	162	56	160	32	8.36	8.88
04:00 PM	172	173	67	175	29	7.31	8.8
05:00 PM	173	167	68	164	28	5.67	8.39

Table 4 Experimental results under Bad day light condition.

Time	LDR-1	LDR-2	LDR-3	LDR-4	Temp (°c)	Fixed panel (W)	Dual Axis panel (W)
07:00 AM	220	216	212	219	20	0.706	2.195
08:00 AM	201	196	197	195	21	1.177	2.878
09:00 AM	46	70	177	67	20	2.173	3.053
10:00 AM	46	66	177	93	20	2.377	3.18
11:00 AM	45	76	177	87	22	2.578	3.067
12:00 PM	180	131	110	130	22	2.863	3.45
01:00 PM	185	65	145	115	23	2.878	3.36
02:00 PM	170	159	54	160	23	2.8	3.277
03:00 PM	173	161	53	159	22	2.713	3.2
04:00 PM	181	172	54	174	22	2.388	3.179
05:00 PM	235	230	236	225	20	1.828	3.032

5.2 Under normal day light condition

The experimental findings obtained under typical day light conditions to evaluate the performance of a fixed and dual axis solar panel of the autonomous solar tracking system are shown in Table 3. The voltage output of each LDR changes from one another as the intensity of light varies from east to west, as evidenced by the measured measurements. Table 3 shows that LDR1 gives low resistance from 7:00 a.m. to 1:00 p.m., whereas LDR3 provides medium resistance from 7:00 a.m. to 11:00 a.m. LDR 2 and LDR 4 give similar resistance from 7:00 a.m. to 1:00 p.m. Fixed panels produce the most from 11:00 a.m. to 3:00 p.m., but the automatic tracking system panel has efficiency of 61 percent, 93 percent, and 82 percent at 7:00 a.m., 12 p.m., and 5:00 p.m., respectively.

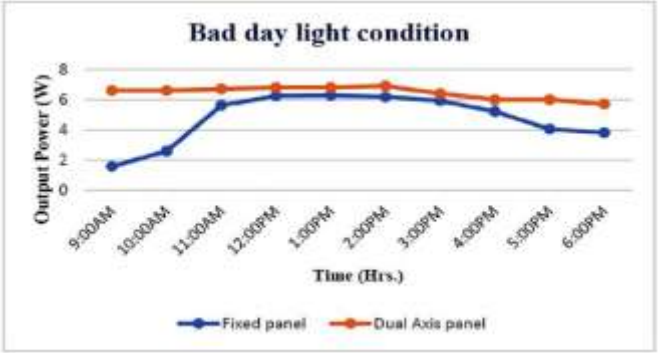

Fig- 5.1 Variations in Output Power during Bad Day Light Condition.

International Journal of Advances in Engineering and Management (IJAEM)
Volume 3, Issue 9 Sep 2021, pp: 654-671 www.ijaem.net ISSN: 2395-5252

The daily average temperature was 28 degrees Celsius. Figure 5.1 depicts the fluctuations in output power during regular daytime lighting conditions.

5.3 Bad day light condition

There's also a collection of readings recorded in low-light conditions below. The light intensity was quite low, resulting in a low PV system output. Table 4 shows the experimental results obtained under poor lighting conditions. From Table 4, it can be deduced that

CONCLUSIONS

The major goal of this project was to exhibit and categorise several types of solar tracking systems according to their technology and driving ways. Active and passive solar tracking systems are the two most common types of solar tracking systems. Active solar tracking systems operate photovoltaic modules with gears and motors, whereas passive tracking systems employ a low-boiling-point compressed gas fluid generated by solar heat. Based on the driving mechanisms used, this study divided active solar tracking systems into five types. Sensor driver systems, microprocessor driver systems, open–closed loop driver systems, intelligent driver systems, and a mix of two or more of these driver systems are the five categories. Intelligent driver systems are the most promising of these tracking systems because they can use machine learning algorithms to forecast the exact location of the sun. As a result, most tracking systems now emphasise the use of intelligent concepts. In the meantime, numerous new efficient solar tracking systems will be devised and implemented in the future based on intelligent concepts.

In the context of future Space Situational Awareness and Space Traffic Management activities, the increasingly frequent launches of satellite constellations and clusters, with special focus to tiny satellite platforms, necessitate more precise and rapid monitoring systems. Satellites can be visually followed throughout the eclipse phase if active illumination payloads such as Light-Emitting Diodes-based boards are used, removing the constraints of light conditions and Sun phase angle.

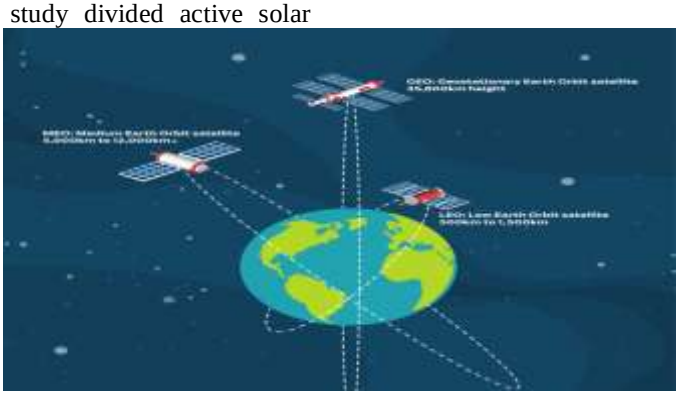

Fig- 5.3 satellite throughout its orbital career

LED payloads can help follow a satellite throughout its orbital career, from early detection in a big cluster to orbit determination, attitude reconstruction, backup light communication, and assistance with Post-Mission Disposal duties. In order to include small telescope stations in the ground segment, the design of an LED-based optical tracking system should take into account the maximisation of irradiance, as allowed by power and available volume restrictions. If using commercial LEDs, the spaceborne LED-based system can use between 15 and 40 diodes (to maximise Quantum Efficiency and irradiance).

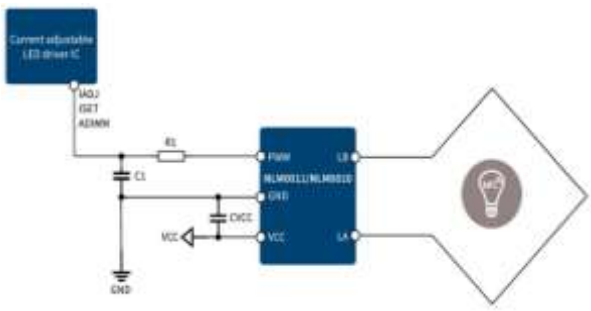

Fig- 5.4 Light Emitting Diode Board

International Journal of Advances in Engineering and Management (IJAEM)
Volume 3, Issue 9 Sep 2021, pp: 654-671 www.ijaem.net ISSN: 2395-5252

Electrical power systems for nano-satellite platforms must adhere to the maximum permissible power limitations. By utilising a tiny part (5%) of the energy generated by a standard 1U Cube Sat EPS, the diodes could perform identifier patterns for recognition and orbit determination every 25-30 seconds. Because of its low energy consumption, the LED system is compatible with the smallest Cube Sat platform, a 1U satellite, as well as the use of LEDs as a supplementary tracking system. Telescopes with relatively low-cost hardware can be considered for the ground section. The observational strategies include moving the telescopes at a sidereal rate, obtaining the satellite LED signal as a strike against the stellar background, or following the target and keeping it in the field of view for the entire pass.

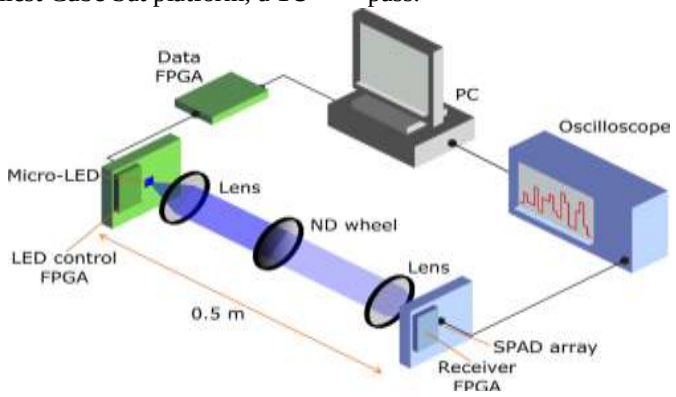

Fig- 5.5 Schematic of the laboratory-based experimental setup.

Single element (CCD and CMOS) and arrayed (CCD and CMOS) (P-I-N or APD photodiodes) Sensors can be used for a variety of purposes, each with its own set of benefits and cons. While photodiodes can be used to deduce flight data from the execution of flashes, CCD or CMOS-based approaches can offer tracking and attitude data. The minimum elevation and atmospheric transmittance at the LEDs flashing wavelength, as well as the ground segment features, are the most restricting criteria to consider when determining the optical link budget. For example, the sensor's characteristics and the observation technique chosen. For data collecting from the ground, a minimum SNR of 10 and a minimum elevation of 20 degrees might be used as standards. While flashing patterns can be improved for a variety of objectives, the most fundamental LED flashing rule is to use both long and short flashes to distinguish the satellite above the background stellar field and reconstruct the target celestial coordinates. Orthogonal patterns, such as Gold codes, can help in simultaneous pattern recognition and attitude determination by discriminating between the different satellite sides flashing with different patterns. When permitting simultaneous observations with colour filters from numerous sensors and/or places, the use of LEDs in different colours can provide an additional benefit. For this research, the LEDSAT 1U CubeSat was employed as a case study. By integrating LEDs in three different bandwidths on all of the spacecraft's sides, the satellite will examine the performance of an LED-based payload. During its mission, the spacecraft will perform early recognition, orbit determination, attitude determination, and backup light-based communication duties. The satellite will be launched in the first quarter of 2021.

REFERENCES

[1]. Best Research-Cell Efficiency Chart. NREL, 2019. [Online]. Available: https://www.nrel.gov/pv/cell-efficiency.html.

[2]. W.A. Badawy, A review on solar cells from Si-single crystals to porous materials and quantum dots, J. Adv. Res. 6(2) (2015) 123–132.

[3]. K. Yoshikawa, H. Kawasaki, W. Yoshida, T. Irie, K. Konishi, K. Nakano, T. Uto, D. Adachi, M. Kanematsu, H. Uzu, K. Yamamoto, Silicon heterojunction solar cell with interdigitated back contacts for a photoconversion efficiency over 26%, Nat. Energy 2(5) (2017) 17032.

[4]. R.W. MacQueen, M. Liebhaber, J. Niederhausen, M. Mews, C. Gersmann, S. Jäckle, K. Jäger, M.J. Tayebjee, T.W. Schmidt, B. Rech, K. Lips, Crystalline siliconsolar cells with tetracene interlayers: The path to silicon-singlet fission heterojunction devices, Mater. Horiz. 5(6) (2018) 1065–1075.

[5]. W. Shockley, H.J. Queisser, Detailed balance limit ofefficiency of pn junction solar cells, J. Appl. Phys. 32(3) (1961) 510–519.

[6]. J. Benick, A. Richter, R. Müller, H. Hauser, F. Feldmann, P.Krenckel, S. Riepe, F. Schindler, M.C. Schubert, M. Hermle, A.W. Bett, High-efficiency n-type HP mc silicon solar cells, IEEE J. Photovolt. 7(5) (2017) 1171–1175.

[7]. F. Meillaud, A. Shah, C. Droz, E. Vallat-Sauvain, C. Miazza, Efficiency limits for single-

junction and tandem solar cells, Sol. Energy Mater. Sol. Cells 90(18–19) (2006) 2952–2959.
[8]. M. Nayfeh, Advanced and low cost energy and lighting devices, Fundam. Appl. Nano Silicon Plasmonics Fullerines (2018) 363–429.
[9]. T. Matsui, K. Maejima, A. Bidiville, H. Sai, T. Koida, T. Suezaki, M. Matsumoto, K. Saito, I. Yoshida, M. Kondo, High-efficiency thin-film silicon solar cells realized by integrating stable a-Si:H absorbers into improved device design, Japanese J. Appl. Phys. 54(8S1) (2015) 08KB10.
[10]. M.A. Green, K. Emery, Solar cell efficiency tables (version 3), Prog. Photovolt. Res. Appl. 2(1) (1994) 27–34.
[11]. S. De Wolf, J. Holovsky, S.J. Moon, P. Löper, B. Niesen, M. Ledinsky, F.J. Haug, J.H. Yum, C. Ballif, Organometallic halide perovskites: Sharp optical absorption edge and its relation to photovoltaic performance, J. Phys. Chem. Lett. 5(6) (2014) 1035–1039.
[12]. Q. Jiang, Z. Chu, P. Wang, X. Yang, H. Liu, Y. Wang, Z. Yin, J. Wu, X. Zhang, J. You, Planar-structure perovskite solar cells with efficiency beyond 21%, Adv. Mater. 29(46) (2017) 1703852.
[13]. Oxford PV, Oxford PV Perovskite Solar Cell Achieves 28% Efficiency, 2018. [Online]. Available: https://www.oxfordpv.com/news/oxford-pv-perovskite-solarcell- achieves-28-efficiency. Accessed on: Apr. 16, 2019.
[14]. S.P. Philipps, F. Dimroth, A.W. Bett, High-efficiency III–V multijunction solar cells, in McEvoy's Handbook of Photovoltaics. Amsterdam, The Netherlands: Elsevier, 2018, pp. 439–472.
[15]. F. Dimroth, M. Grave, P. Beutel, U. Fiedeler, C. Karcher, T.N. Tibbits, E. Oliva, G. Siefer, M. Schachtner, A. Wekkeli, A.W. Bett, Wafer bonded four-junction GaInP/GaAs//GaInAsP/GaInAs concentrator solar cells with 44.7% efficiency, Prog. Photovolt. Res. Appl. 22(3) (2014) 277–282.
[16]. H. Helmers, O. Höhn, D. Lackner, E. López, L. Ruiz-Preciado, M. Schauerte, G. Siefer, F. Dimroth, A.W. Bett, Highly efficient III-V based photovoltaic laser power converter, in 1st Optical Wireless and Fiber Power Transmission Conf. (OWPT2019), no. OWPT-1-01, Yokohama, Japan, 2019.
[17]. J.F. Geisz, R.M. France, K.L. Schulte, M.A. Steiner, A.G. Norman, H.L. Guthrey, M.R. Young, T. Song, T. Moriarty, Six-junction III–V solar cells with 47.1% conversion efficiency under 143 Suns concentration, Nat. Energy 5(4) (2020) 326–335.
[18]. Luo Y, Zhang L, Wang X, Xie L, Liu ZB, Wu J, et al. A comparative study on thermal performance evaluation of a new double skin façade system integrated with photovoltaic blinds. Appl Energy 2017;199(8):281–93.
[19]. Hu Z, He W, Ji J, Hu DY, Lv S, Chen HB, et al. Comparative study on the annual performance of three types of building integrated photovoltaic (BIPV) Trombe wall system. Appl Energy 2017;194(5):81–93.
[20]. Li L, Qu M, Peng S. Performance evaluation of building integrated solar thermal shading system: building energy consumption and daylight provision. Energy Build 2016;113:189–201.
[21]. Jung HY, Kim KS. Control strategy of a venetian blind for visual improvement of work plane. J Archit Inst Korea 2010;26(12):279–86.
[22]. Huang Y, Niu JL, Chung TM. Comprehensive analysis on thermal and daylighting performance of glazing and shading designs on office building envelope in cooling dominant climates. Appl Energy 2014;134:215–28.
[23]. Koo SY, Yeo MS, Kim KW. Automated blind control to maximize the benefits of daylight in buildings. Build Environ 2010;45:1508–20.
[24]. Tzempelikos A. The impact of venetian blind geometry and tilt angle on view, direct light transmission and interior illuminance. Sol Energy 2008;82:1172–91.
[25]. Hong S, Choi AS, Sung M. Development and verification of a slat control method for a bi-directional PV blind. Appl Energy 2017;206(6):1321–33.
[26]. Roche L. Summertime performance of an automated lighting and blinds control system. Light Res Technol 2002;34:11–27.
[27]. Kim SH, Kim IT, Choi AS, Sung MK. Evaluation of optimized PV power generation and electrical lighting energy savings from the PV blind-integrated daylight responsive dimming system using LED lighting. Sol Energy 2014;107(9):746–57.
[28]. Kang H, Hong T, Jung S, Lee M. Techno-economic performance analysis of the smart solar photovoltaic blinds considering the photovoltaic panel type and the solar tracking method. Build Environ 2019;193(6):1–14. tracking shading elements towards maximum power generation and non-glare daylighting. Appl Energy 2018;228:1454–72.
[29]. Jayathissa P, Luzzatto M, Schmidli J, Hofer J, Nagy Z, Schlueter A, et al. Optimising building

net energy demand with dynamic BIPV shading. Appl Energy2017;202(9):726–35.

[30]. Mousazadeh H, Keyhani A, Javadi A, Mobli H, Abrinia K, Sharifi A. A review of principle and sun-tracking methods for maximizing solar systems output. Renew Sustain Energy Rev 2009;13(8):1800–18.

[31]. Gao Y, Dong JF, Isabella O, Santbergen R, Tan H, Zeman M, et al. A photovoltaic window with sun-